

# Model independent extraction of the proton charge radius from electron scattering

RICHARD J. HILL AND GIL PAZ

*Enrico Fermi Institute and Department of Physics  
The University of Chicago, Chicago, Illinois, 60637, USA*

## Abstract

Constraints from analyticity are combined with experimental electron-proton scattering data to determine the proton charge radius. In contrast to previous determinations, we provide a systematic procedure for analyzing arbitrary data without model-dependent assumptions on the form factor shape. We also investigate the impact of including electron-neutron scattering data, and  $\pi\pi \rightarrow N\bar{N}$  data. Using representative datasets we find  $r_E^p = 0.870 \pm 0.023 \pm 0.012$  fm using just proton scattering data;  $r_E^p = 0.880_{-0.020}^{+0.017} \pm 0.007$  fm adding neutron data; and  $r_E^p = 0.871 \pm 0.009 \pm 0.002 \pm 0.002$  fm adding  $\pi\pi$  data. The analysis can be readily extended to other nucleon form factors and derived observables.

# 1 Introduction

The electromagnetic form factors of the nucleon provide basic inputs to precision tests of the Standard Model. In particular, the root mean square (RMS) proton charge radius as determined by the form factor slope<sup>1</sup>,

$$G_E^p(q^2) = 1 + \frac{q^2}{6} \langle r^2 \rangle_E^p + \dots, \quad (1)$$

is an essential input to hydrogenic bound state calculations [1, 2]. Recent experimental results suggest a discrepancy between the charge radius inferred from the Lamb shift in muonic hydrogen [3],  $r_E^p \equiv \sqrt{\langle r^2 \rangle_E^p} = 0.84184(67)$  fm, and the CODATA value,  $r_E^p = 0.8768(69)$  fm, extracted mainly from (electronic) hydrogen spectroscopy [4]. The charge radius can also be extracted from elastic electron-proton scattering data. The 2010 edition of the Review of Particle Physics lists 12 such determinations that span the range of 0.8-0.9 fm [5], most with quoted uncertainties of 0.01-0.02 fm. These determinations correspond to analyses of different datasets and different functional forms of  $G_E^p(q^2)$  that were fit to the data over a period of 50 years.

Extraction of the proton charge radius from scattering data is complicated by the unknown functional behavior of the form factor. We are faced with the tradeoff between introducing too many parameters (which limits predictive power) and too few parameters (which biases the fits). Here we describe a procedure that provides model-independent constraints on the functional behavior of the form factor. The constraints make use of the known analytic properties of the form factor, viewed as a function of the complex variable  $t = q^2 = -Q^2$ .

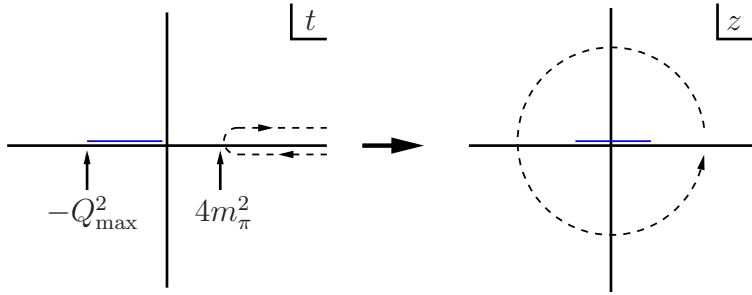


Figure 1: Conformal mapping of the cut plane to the unit circle.

As illustrated in figure 1, the form factor is analytic outside of a cut at timelike values of  $t$ , [6] beginning at the two-pion production threshold,  $t \geq 4m_\pi^2$ .<sup>2</sup> In a restricted region of physical kinematics accessed experimentally,  $-Q_{\max}^2 \leq t \leq 0$ , the distance to singularities implies the existence of a small expansion parameter. We begin by performing a conformal

<sup>1</sup> $G_E^p$  is defined in Section 3.1.

<sup>2</sup> Here and throughout,  $m_\pi = 140$  MeV denotes the charged pion mass, and  $m_N = 940$  MeV is the nucleon mass.

mapping of the domain of analyticity onto the unit circle:

$$z(t, t_{\text{cut}}, t_0) = \frac{\sqrt{t_{\text{cut}} - t} - \sqrt{t_{\text{cut}} - t_0}}{\sqrt{t_{\text{cut}} - t} + \sqrt{t_{\text{cut}} - t_0}}, \quad (2)$$

where for this case  $t_{\text{cut}} = 4m_\pi^2$ , and  $t_0$  is a free parameter representing the point mapping onto  $z = 0$ . By the choice  $t_0^{\text{opt}} = t_{\text{cut}} \left(1 - \sqrt{1 + Q_{\text{max}}^2/t_{\text{cut}}}\right)$ , the maximum value of  $|z|$  is minimized:  $|z| \leq |z|_{\text{max}} = [(1 + Q_{\text{max}}^2/t_{\text{cut}})^{\frac{1}{4}} - 1]/[(1 + Q_{\text{max}}^2/t_{\text{cut}})^{\frac{1}{4}} + 1]$ . For example, with  $Q_{\text{max}}^2 = 0.05 \text{ GeV}^2, 0.5 \text{ GeV}^2$ , we find  $|z|_{\text{max}} = 0.062, 0.25$ . Expanding the form factor as

$$G_E^p(q^2) = \sum_{k=0}^{\infty} a_k z(q^2)^k, \quad (3)$$

we find that the impact of higher order terms are suppressed by powers of this small parameter<sup>3</sup>. As we will see below, the coefficients multiplying  $z^k$  are bounded in size, guaranteeing that a finite number of parameters are necessary to describe the form factor with a given precision. Figure 2 illustrates the manifestation of this fact in the form factor data. As expected, the curvature is smaller in the  $z$  variable than in the  $Q^2$  variable.

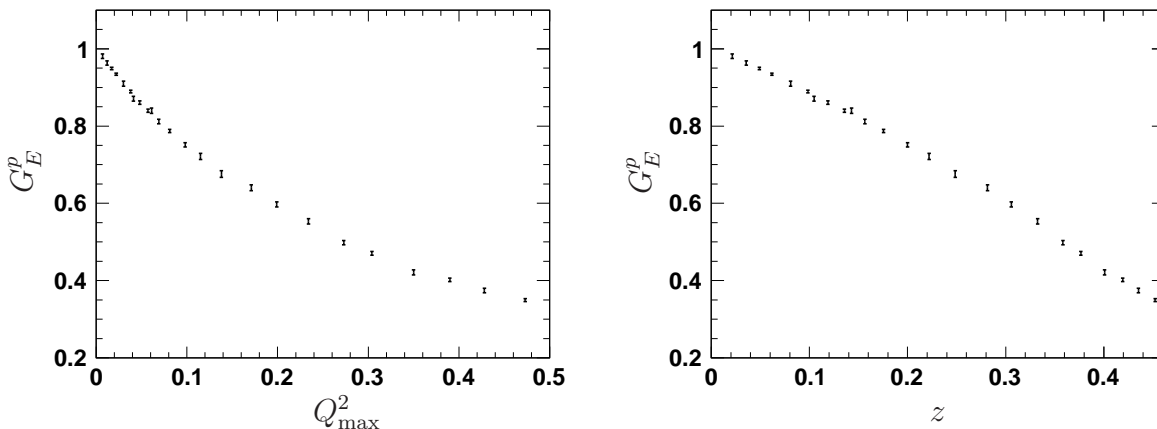


Figure 2: Form factor as a function of  $Q^2$  and as a function of  $z$ . Here we choose  $t_0 = 0$  in the definition of  $z$ , and plot data from [7] for  $0 \leq Q^2 \leq 0.5 \text{ GeV}^2$ .

Expansions of the form (2) are a standard tool in analyzing meson transition form factors [8, 9, 10, 11, 12, 13, 14, 15, 16, 17, 18]. A complicating feature in the present application to nucleon form factors is the contribution of the subthreshold region  $4m_\pi^2 \leq t \leq 4m_N^2$  in the relevant dispersion integral.

The rest of the paper is structured as follows. In Section 2 we demonstrate the application of the  $z$  expansion in some illustrative fits and compare it to other expansions that appear in

<sup>3</sup> Physical observables are independent of the choice of  $t_0$ , which can be viewed as the choice of an expansion “scheme”.  $|z|_{\text{max}}$  defined in this way gives a convenient estimation of the impact of higher-order terms.

the literature. One of the main advantages of the  $z$  expansion is that the expansion coefficients can be bounded using knowledge about  $\text{Im}G_E^p$  in the time-like region. In Section 3 we discuss these bounds. In Section 4 we discuss several possibilities of reducing the error on the charge radius by including more experimental data, namely: high  $Q^2$  data, neutron scattering data, and  $\pi\pi$  data. Finally, we discuss our results in Section 5.

## 2 Illustrative fits

Let us consider the six datasets tabulated by Rosenfelder [19] (denoted in [19] as S1, S2, R, B1, B2, M) This will allow us to compare in detail the results of our fit to previous analyses. For definiteness, we take all data points in [19] with corrections from magnetic form factor contributions  $\Delta_{\text{mag}} \leq 0.15$ . The resulting dataset has 85 points with  $Q^2 \lesssim 0.04 \text{ GeV}^2$ .

We will fit to three types of parameterization. The first is a simple Taylor series expansion,

$$G_E^p(q^2) = 1 + a_1 \frac{q^2}{t_{\text{cut}}} + a_2 \left( \frac{q^2}{t_{\text{cut}}} \right)^2 + \dots, \quad (4)$$

where we choose to work in units  $t_{\text{cut}} = 4m_\pi^2$ . The second is a continued fraction expansion put forward in [20],

$$G_E^p(q^2) = \frac{1}{1 + a_1 \frac{q^2/t_{\text{cut}}}{1 + a_2 \frac{q^2/t_{\text{cut}}}{1 + \dots}}} = 1 - a_1 \frac{q^2}{t_{\text{cut}}} + (a_1 a_2 + a_1^2) \left( \frac{q^2}{t_{\text{cut}}} \right)^2 + \dots. \quad (5)$$

We are not aware of a motivation for this ansatz from first principles, but it has been used to obtain one of the widely quoted values of the proton charge radius from electron scattering. The third is the  $z$  expansion described in the Introduction,

$$G_E^p(q^2) = 1 + a_1 z(q^2) + a_2 z^2(q^2) + \dots = 1 - \frac{a_1}{4} \frac{q^2}{t_{\text{cut}}} + \left( -\frac{a_1}{8} + \frac{a_2}{16} \right) \left( \frac{q^2}{t_{\text{cut}}} \right)^2 + \dots, \quad (6)$$

where  $z(q^2) = z(q^2, t_{\text{cut}}, t_0 = 0)$ . As explained below, the coefficients in this expansion are bounded; for definiteness here we take  $|a_k| \leq 10$ .

We perform fits by minimizing a  $\chi^2$  function,

$$\chi^2 = \sum_{i,j} (\text{data}_i - \text{theory}_i) E_{ij}^{-1} (\text{data}_j - \text{theory}_j), \quad (7)$$

where the error matrix is formed by adding in quadrature the quoted statistical errors, assumed uncorrelated, and normalization error, assumed fully correlated within each dataset. In the notation of Table 1 of Ref. [19] we use for each experiment, (note that  $\delta_{\text{norm}}$  refers to the error in the *cross section*)<sup>4</sup>

$$E_{ij} = (\delta G_E)_i^2 \delta_{ij} + (\delta_{\text{norm}}/2)^2 (G_E)_i (G_E)_j. \quad (8)$$

---

<sup>4</sup> We obtain similar results by floating the normalization of each experiment and constraining the scale factors by an additional contribution to  $\chi^2$  (as done in [19]) or by performing the fits at fixed (unit) normalization and assigning an additional error obtained by adding in quadrature the shift induced by redoing the fits with shifted normalization (as done in [20]).

	$k_{\max} = 1$	2	3	4	5
polynomial	$836_{-9}^{+8}$	$867_{-24}^{+23}$	$866_{-56}^{+52}$	$959_{-93}^{+85}$	$1122_{-137}^{+122}$
	$\chi^2=34.49$	32.51	32.51	31.10	28.99
continued fraction	$882_{-10}^{+10}$	$869_{-25}^{+26}$	—	—	—
	$\chi^2=32.81$	32.51			
$z$ expansion (no bound)	$918_{-9}^{+9}$	$868_{-29}^{+28}$	$879_{-69}^{+64}$	$1022_{-114}^{+102}$	$1193_{-174}^{+152}$
	$\chi^2=36.14$	32.52	32.48	30.35	28.92
$z$ expansion ( $ a_k  \leq 10$ )	$918_{-9}^{+9}$	$868_{-29}^{+28}$	$879_{-59}^{+38}$	$880_{-61}^{+39}$	$880_{-62}^{+39}$
	$\chi^2=36.14$	32.52	32.48	32.46	32.45

Table 1: Proton charge radius extracted from data of Table 1 of [19] ( $Q^2 \lesssim 0.04 \text{ GeV}^2$ ) in units of  $10^{-18}$  m, using different functional behaviors of the form factor. Dashes denote fits that do not constrain the slope to be positive.

Errors for the form factor slope are computed by finding the  $\Delta\chi^2 = 1$  range<sup>5</sup>.

As can be seen from Table 1, the fits with one free parameter differ by many standard deviations. Fits with two free parameters agree well, while fits with three or more parameters become increasingly unconstrained for the polynomial and continued fraction expansions, as well as for the  $z$  expansion when no constraints on the expansion coefficients are in place. In particular, for  $k_{\max} \geq 3$  in the continued fraction expansion, no meaningful fit can be performed (e.g., the slope is not constrained to be positive).

These results illustrate the problem to be addressed: without detailed knowledge of the functional behavior of the form factor, we risk using either too few parameters and biasing the fit; or too many parameters and losing predictive power. Note that performing trial fits on model data as in [20] is also problematic; some assumption must be made on the functional behavior of the form factor in creating the model datasets. To make model independent statements requires identifying a bounded class of functions that is guaranteed to contain the true form factor, yet is sufficiently restrictive to retain predictive power. The following section describes such a class of functions.

### 3 Dispersive bounds

The above fit to the  $z$  expansion with a bound on the coefficients illustrates our basic methodology. The present section justifies the  $|a_k| \leq 10$  bound, and demonstrates how further constraints can be obtained by disentangling the isoscalar and isovector components of the form factor.

---

<sup>5</sup> We have performed these computations in both MAPLE and MATHEMATICA, and have also checked our results using MINOS errors in MINUIT.

### 3.1 Form factor definitions

For completeness we list definitions of the various form factors. The Dirac and Pauli form factors,  $F_1^N$  and  $F_2^N$ , respectively, are defined by [21, 22]

$$\langle N(p') | J_\mu^{\text{em}} | N(p) \rangle = \bar{u}(p') \left[ \gamma_\mu F_1^N(q^2) + \frac{i\sigma_{\mu\nu}}{2m_N} F_2^N(q^2) q^\nu \right] u(p), \quad (9)$$

where  $q^2 = (p' - p)^2 = t$  and  $N$  stands for  $p$  or  $n$ . The Sachs electric and magnetic form factors are related to the Dirac-Pauli basis by [23]

$$G_E^N(t) = F_1^N(t) + \frac{t}{4m_N^2} F_2^N(t), \quad G_M^N(t) = F_1^N(t) + F_2^N(t). \quad (10)$$

At  $t = 0$  they are [5]  $G_E^p(0) = 1$ ,  $G_E^n(0) = 0$ ,  $G_M^p(0) = \mu_p \approx 2.793$ ,  $G_M^n(0) = \mu_n \approx -1.913$ . We write the isoscalar and isovector form factors as

$$G_E^{(0)} = G_E^p + G_E^n, \quad G_E^{(1)} = G_E^p - G_E^n, \quad (11)$$

such that at  $t = 0$  they are,  $G_E^{(0)}(0) = 1$ ,  $G_E^{(1)}(0) = 1$ ,  $G_M^{(0)}(0) = \mu_p + \mu_n$ ,  $G_M^{(1)}(0) = \mu_p - \mu_n$ . Notice that  $G_{E,M}^{(0)} = 2G_{E,M}^s$ ,  $G_{E,M}^{(1)} = 2G_{E,M}^v$  for  $G_{E,M}^{s,v}$  of [26].

### 3.2 Dispersive bounds

The analytic structure in the  $t$  plane illustrated in Fig. 1 implies the dispersion relation,

$$G_E^p(t) = \frac{1}{\pi} \int_{t_{\text{cut}}}^{\infty} dt' \frac{\text{Im} G_E^p(t' + i0)}{t' - t}. \quad (12)$$

Knowledge of  $\text{Im} G_E^p$  over the cut translates into information about the coefficients in the  $z$  expansion. We begin with a general discussion of these relations.

Let us consider a general function with the analytic structure as in Fig. 1,  $G(t) = \sum_{k=0}^{\infty} a_k z(t)^k$ . Equation (2) maps points just above (below) the cut in the  $t$  plane onto points in the lower (upper) half unit circle in the  $z$  plane. Parameterizing the unit circle by  $z(t) = e^{i\theta}$  and solving (2) for  $t$ , we find

$$t = t_0 + \frac{2(t_{\text{cut}} - t_0)}{1 - \cos \theta} \equiv t(\theta). \quad (13)$$

We can now use the orthogonality of  $z^k$  over the unit circle to find

$$a_k = \frac{1}{\pi} \int_0^\pi d\theta \text{Re} G[t(\theta) + i0] \cos(k\theta) - \frac{1}{\pi} \int_0^\pi d\theta \text{Im} G[t(\theta) + i0] \sin(k\theta). \quad (14)$$

Since  $G$  is analytic,  $a_k = 0$  for  $k < 0$ , and therefore

$$a_0 = \frac{1}{\pi} \int_0^\pi d\theta \text{Re} G[t(\theta) + i0] = G(t_0),$$

$$a_k = -\frac{2}{\pi} \int_0^\pi d\theta \text{Im} G[t(\theta) + i0] \sin(k\theta) = \frac{2}{\pi} \int_{t_{\text{cut}}}^{\infty} \frac{dt}{t - t_0} \sqrt{\frac{t_{\text{cut}} - t_0}{t - t_{\text{cut}}}} \text{Im} G(t) \sin[k\theta(t)], \quad k \geq 1. \quad (15)$$

		$t_0 = 0$	$t_0 = t_0^{\text{opt}}(0.5 \text{ GeV}^2)$
$\phi = 1$	$\ G_E^{(0)}\ _2/G_E^{(0)}(t_0)$	7.6	12.1
	$\ G_E^{(1)}\ _2/G_E^{(1)}(t_0)$	2.5	3.9
$\phi = \phi_{\text{OPE}}$	$\ \phi^{(0)}G_E^{(0)}\ _2/\phi^{(0)}(t_0)G_E^{(0)}(t_0)$	14.4	23.5
	$\ \phi^{(1)}G_E^{(1)}\ _2/\phi^{(1)}(t_0)G_E^{(1)}(t_0)$	4.6	6.7
$\phi = 1$	$2\sqrt{\frac{t_{\text{cut}}-t_0}{m_V^2-t_{\text{cut}}}}_{I=0}$	1.3	1.8
	$2\sqrt{\frac{t_{\text{cut}}-t_0}{m_V^2-t_{\text{cut}}}}_{I=1}$	0.78	1.3

Table 2: Typical bounds on the coefficient ratios  $\sqrt{\sum_k a_k^2/a_0^2}$  (upper part of table) and  $|a_k/a_0|$  (lower part) in a vector dominance ansatz.  $\phi_{\text{OPE}}$  is defined in Eq.(23).

The coefficients in the expansion (3) can also be used to construct a norm of the form factor in the mathematical sense. To keep the discussion general, let us introduce a function  $\phi$  sharing the domain of analyticity of  $G$ , and write

$$\phi G = \sum_{k=0}^{\infty} a_k z^k. \quad (16)$$

Consider the class of norms specified by

$$\|\phi G\|_p = \left( \sum_k |a_k|^p \right)^{\frac{1}{p}}. \quad (17)$$

In particular, the “uniform norm” is equal to the maximum coefficient size,  $\|\phi G\|_{\infty} = \sup_k |a_k| = \lim_{p \rightarrow \infty} \|\phi G\|_p$ . The case  $p = 2$  is of special interest since the norm is easily related to a dispersion integral,

$$\|\phi G\|_2 = \left( \sum_k a_k^2 \right)^{\frac{1}{2}} = \left( \oint \frac{dz}{z} |\phi G|^2 \right)^{\frac{1}{2}} = \left( \frac{1}{\pi} \int_{t_{\text{cut}}}^{\infty} \frac{dt}{t-t_0} \sqrt{\frac{t_{\text{cut}}-t_0}{t-t_{\text{cut}}}} |\phi G|^2 \right)^{\frac{1}{2}}. \quad (18)$$

The finiteness of  $\|\phi G\|_2$  shows that the coefficients  $a_k$  are not only bounded, but must *decrease* in size for sufficiently large  $k$ . The relation  $\|\phi G\|_{\infty} \leq \|\phi G\|_2$  indicates that  $\|\phi G\|_2$  may overestimate the actual size of the relevant coefficients in certain cases. We proceed to consider a vector dominance model to illustrate this feature and then turn to a more detailed analysis of the spectral functions.

### 3.3 Vector dominance ansatz

In many applications, the  $\|\cdot\|_2$  norm is used in conjunction with “unitarity bounds” obtained by identifying the dispersive integral with a physical production rate. In the present example,

dominant contributions to the integral arise from the region below the two-nucleon production threshold, and we must turn to different methods of analysis. For example, employing a vector dominance ansatz in the appropriate channel, Table 2 displays estimates for the quantity  $\|\phi G\|_2/\phi(t_0)G(t_0) = \sqrt{\sum_k a_k^2/a_0^2}$ , for different choices of the functional form of  $\phi$  and the value of  $t_0$ <sup>6</sup>. The effects of the leading resonance in each channel are represented by a Breit Wigner profile [24],

$$F_i^{(I=0)} \sim \frac{\alpha_i m_\omega^2}{m_\omega^2 - t - i\Gamma_\omega m_\omega}, \quad F_i^{(I=1)} \sim \frac{\beta_i m_\rho^2}{m_\rho^2 - t - i\Gamma_\rho m_\rho}, \quad (19)$$

with  $\alpha_1 \approx 1$ ,  $\alpha_2 \approx -0.12$ ,  $m_\omega = 783$  MeV,  $\Gamma_\omega = 8.5$  MeV for the isoscalar channel; and  $\beta_1 \approx 1$ ,  $\beta_2 \approx 3.7$ ,  $m_\rho = 775$  MeV,  $\Gamma_\rho = 149$  MeV for the isovector channel. At  $\Gamma = 0$ , the ansatz is normalized to the  $t = 0$  values in Section 3.1.

We note that in the isoscalar case, the rather large size of the estimated norm is due to the narrow width of the  $\omega$  resonance; in fact, in the limit of an infinitely narrow resonance, the quantity  $\|G\|_2$  diverges, as seen from (18). Closer examination indicates that the large norm is due not to the coefficients growing in size, but rather to a sequence of coefficients whose slow fall-off causes a slow convergence for the sum  $\sum_k a_k^2$ . A straightforward computation shows that the expansion coefficients for an infinitely narrow pole,  $G(t) = G(0)/(1 - t/m_V^2)$ , are for  $k \geq 1$ ,

$$\frac{a_k}{a_0} = -2\sqrt{\frac{t_{\text{cut}} - t_0}{m_V^2 - t_{\text{cut}}}} \sin \left[ 2k \arcsin \left( \sqrt{\frac{t_{\text{cut}} - t_0}{m_V^2 - t_0}} \right) \right]. \quad (20)$$

In particular,  $|a_k/a_0| \leq 2\sqrt{(t_{\text{cut}} - t_0)/(m_V^2 - t_{\text{cut}})}$ . This approximation to the uniform norm is also displayed in Table 2.

Equations (15) and (18) are model-independent, whereas the approximations based on the vector dominance ansatz employed in Table 2 are model dependent. This ansatz aims simply to capture the order of magnitude of the coefficients, which is sufficient in practice to constrain the form factor fits. The conclusion is that  $|a_k| \leq 10$  is a very conservative estimate for this ansatz.

### 3.4 Explicit $\pi\pi$ continuum

We can be more explicit in the case of the isovector form factor expansion, where the leading singularities are due to  $\pi\pi$  continuum contributions that are in principle constrained by measured  $\pi\pi$  production and  $\pi\pi \rightarrow N\bar{N}$  annihilation rates [6, 25, 26]:

$$\text{Im } G_E^{(1)}(t) = \frac{2}{m_N \sqrt{t}} (t/4 - m_\pi^2)^{\frac{3}{2}} F_\pi(t)^* f_+^1(t), \quad (21)$$

where  $F_\pi(t)$  is the pion form factor (normalized according to  $F_\pi(0) = 1$ ) and  $f_+^1(t)$  is a partial amplitude for  $\pi\pi \rightarrow N\bar{N}$ . Using that these quantities share the same phase [25], we may substitute absolute values. Strictly speaking, this relation holds up to the four-pion threshold,

---

<sup>6</sup> For this purpose we estimate  $G_E(t_0)$  using a dipole ansatz for the form factor,  $G_E(t) \sim 1/(1 - t/0.71 \text{ GeV}^2)^2$ .



$t \leq 16m_\pi^2$ . For the purposes of estimating coefficient bounds, we will take the extension of (21) assuming phase equality through the  $\rho$  peak as a model for the total  $\pi\pi$  continuum contribution.

For  $|F_\pi(t)|$  we take an interpolation using the four  $t$  values close to production threshold from [27] (0.101 to 0.178 GeV<sup>2</sup>), and 43  $t$  values from [28] (0.185 to 0.94 GeV<sup>2</sup>). Values for  $f_+^1(t)$  are taken from Table 2.4.6.1 of [29]. Evaluating (15) using (21) and the experimental data up to  $t = 0.8 \text{ GeV}^2 \approx 40 m_\pi^2$  yields for the first few coefficients, at  $\phi = 1$  and  $t_0 = 0$ :  $a_0 \approx 2.1$ ,  $a_1 \approx -1.4$ ,  $a_2 \approx -1.6$ ,  $a_3 \approx -0.9$ ,  $a_4 \approx 0.2$ . Using  $|\sin(k\theta)| \leq 1$  in the integral gives  $|a_k| \lesssim 2.0$  for  $k \geq 1$ .

The leading singularities in the isoscalar channel could in principle be analyzed using data for the  $3\pi$  continuum. Since we do not attempt to raise the isoscalar threshold in our analysis, we content ourselves with a simple vector dominance model to estimate the coefficient bounds. The first few coefficients for the isoscalar form factor using (20) for a narrow  $\omega$  resonance are:  $a_0 = 1$ ,  $a_1 \approx -1.2$ ,  $a_2 \approx -0.96$ ,  $a_3 \approx 0.4$ ,  $a_4 \approx 1.3$ . We will compare the above values to those extracted from electron scattering data later. For the moment we note that a bound  $|a_k| \leq 10$  is conservative.

### 3.5 Choice of $\phi$

Let us return to the choice of  $\phi$ . We will consider three essentially different choices. First,  $\phi(t) = 1$  is our default choice. We noted that for  $\phi = 1$  the dominant contributions to  $\|\phi G\|_2$  are from narrow resonances. We could negate the large contribution of the leading resonances by using for  $\phi$  the inverse of a vector meson dominance (VMD) form factor. As a second choice, consider

$$\phi_{\text{VMD}}(t) = (m_V^2 - t)/m_V^2, \quad (22)$$

where  $m_V$  is the mass of the leading resonance in the appropriate channel, i.e.,  $\rho(770)$  for the isovector,  $\omega(780)$  for the isoscalar. Note that using  $G_E \sim 1/t^2$  at large  $t$ , the dispersion integral remains convergent. There is no loss of model-independence here, since corrections to vector dominance are accounted for in the coefficients  $a_k$ . As discussed in Section 3.6, a third choice of  $\phi$  is motivated by unitarity and an operator product expansion (OPE):

$$\phi_{\text{OPE}}(t) = \frac{m_N}{\sqrt{6}\pi} \frac{(t_{\text{cut}} - t)^{\frac{1}{4}}}{(t_{\text{cut}} - t_0)^{\frac{1}{4}}} \left[ \frac{z(t, t_{\text{cut}}, 0)}{-t} \right]^{\frac{1}{4}} \left[ \frac{z(t, t_{\text{cut}}, t_0)}{t_0 - t} \right]^{-\frac{1}{2}} \left[ \frac{z(t, t_{\text{cut}}, -Q_{\text{OPE}}^2)}{-Q_{\text{OPE}}^2 - t} \right]^{\frac{3}{2}} (4m_N^2 - t)^{\frac{1}{4}}, \quad (23)$$

where  $t_{\text{cut}}$  is appropriate to the chosen isospin channel. For definiteness, we choose  $Q_{\text{OPE}}^2 = 1 \text{ GeV}^2$  in the unitarity-inspired  $\phi$ . In our final fits, we focus on  $\phi = 1$  and  $t_0 = 0$  but demonstrate that the results are essentially unchanged for different choices.

### 3.6 Bounds on the region $t \geq 4m_N^2$

The contribution of the physical region  $t \geq 4m_N^2$  to  $\|\phi G_E\|_2$  is

$$\delta\|\phi G_E\|_2^2 = \frac{1}{\pi} \int_{4m_N^2}^{\infty} \frac{dt}{t-t_0} \sqrt{\frac{t_{\text{cut}}-t_0}{t-t_{\text{cut}}}} |\phi G_E|^2. \quad (24)$$

The cross section for  $e^+e^- \rightarrow N\bar{N}$  is [30]

$$\sigma(t) = \frac{4\pi\alpha^2}{3t} \sqrt{1 - \frac{4m_N^2}{t}} \left( |G_M(t)|^2 + \frac{2m_N^2}{t} |G_E(t)|^2 \right), \quad (25)$$

and thus for the proton electric form factor we have

$$\delta\|\phi G_E^p\|_2^2 = \frac{1}{\pi} \int_{4m_N^2}^{\infty} \frac{dt}{t-t_0} \sqrt{\frac{t_{\text{cut}}-t_0}{t-t_{\text{cut}}}} |\phi|^2 \left[ \frac{\sigma(t)}{\sigma_0(t)v(t)} \frac{1}{|G_M/G_E|^2 + 2m_N^2/t} \right], \quad (26)$$

where  $\sigma_0 = 4\pi\alpha^2/3t$  and  $v(t) = \sqrt{1 - 4m_N^2/t}$  is the nucleon velocity in the center-of-mass frame. Using the data from [31] (see also [32, 33]), we can perform the integral from  $t = 4.0 \text{ GeV}^2$  to  $9.4 \text{ GeV}^2$  assuming  $|G_M^p/G_E^p| \lesssim 1$ .<sup>7</sup> At  $t_0 = 0$  and  $\phi = 1$ , we find the result  $\delta\|G_E^p\|_2^2 \lesssim (0.03)^2$ , to be added to the contribution from  $t \leq 4m_N^2$ . This result is obtained by using for  $\sigma(t)$  the measured central value plus  $1\sigma$  error. The remaining integral above  $t = 9.4 \text{ GeV}^2$  can be conservatively estimated by assuming a constant form factor beyond this point, yielding an additional  $\delta\|G_E^p\|_2^2 \approx (0.008)^2$ . The neutron form factor can be treated similarly using the data from [34] for  $t = 3.61$  to  $5.95 \text{ GeV}^2$ . This leads to  $\delta\|G_E^n\|_2^2 \approx (0.05)^2$ . The remainder at high  $t$  assuming a constant form factor yields an additional  $\delta\|G_E^n\|_2^2 \approx (0.05)^2$ . Similarly, using  $|\text{Im}G_E \sin k\theta| \leq |G_E|$  the contribution of the timelike region to (15) is small:  $|\delta a_k| \lesssim 0.011 + 0.004$  for the proton, and  $|\delta a_k| \lesssim 0.013 + 0.025$  for the neutron. We conclude that when estimating the bounds on coefficients, the physical timelike region can be safely neglected.

Let us mention that we can bound the contribution of the physical timelike region by a perturbative quark-level computation. Decompose the electromagnetic current correlation function as

$$\Pi^{\mu\nu}(q) = i \int d^4x e^{iq \cdot x} \langle 0 | T \{ J_{\text{em}}^\mu(x), J_{\text{em}}^\nu(0) \} | 0 \rangle = (q^\mu q^\nu - q^2 g^{\mu\nu}) \Pi(q^2). \quad (27)$$

and define

$$\chi(Q_{\text{OPE}}^2) = \frac{1}{2} \frac{\partial^2}{\partial(q^2)^2} (q^2 \Pi(q^2)) \Big|_{q^2 = -Q_{\text{OPE}}^2} = \frac{1}{\pi} \int_{t_0}^{\infty} dt \frac{t \text{Im}\Pi(t)}{(t + Q_{\text{OPE}}^2)^3}. \quad (28)$$

The two-nucleon contribution to the correlator satisfies

$$\text{Im}\Pi(t) \geq \frac{m_N^2}{6\pi t} \sqrt{1 - \frac{4m_N^2}{t}} |\phi G_E|^2, \quad (29)$$

---

<sup>7</sup> For  $|G_M/G_E| \geq 1$ , the quantity in square brackets in (26) is bounded by the quantity denoted by  $|G|^2$  in [31]. This inequality is satisfied experimentally in the  $t$  range of interest.

and hence with  $\phi G_E = \sum_k a_k z^k$  and the choice of  $\phi$  in (23),

$$\chi(Q_{\text{OPE}}^2) \geq \frac{1}{\pi} \int_{4m_N^2}^{\infty} \frac{dt}{t-t_0} \sqrt{\frac{t_{\text{cut}}-t_0}{t-t_{\text{cut}}}} |\phi G_E|^2 \geq \delta \|\phi G_E\|_2^2. \quad (30)$$

If we choose  $Q_{\text{OPE}}^2$  large enough, the function  $\chi(Q_{\text{OPE}}^2)$  is perturbatively calculable as an operator product expansion:  $\chi \approx \sum_f e_f^2 / 8\pi^2 Q_{\text{OPE}}^2$  at leading order, where  $e_f$  denotes the electric charge of a given quark flavor. Choosing for illustration  $Q_{\text{OPE}}^2 = 1 \text{ GeV}^2$ ,  $n_f = 3$  light quark flavors, and  $t_{\text{cut}} = 4m_\pi^2$ , we find the bounds  $\delta(\sum_k a_k^2) \sim (1.0)^2$  for  $t_0 = 0$  and  $\delta(\sum_k a_k^2/a_0^2) \sim (1.4)^2$  for  $t_0 = t_0^{\text{opt}}(0.5 \text{ GeV}^2)$ . We note that these ‘‘unitarity bounds’’ overestimate the contribution from the physical region  $t \geq 4m_N^2$ , due both to subthreshold resonance production, and to other channels, e.g.,  $N\bar{N}$  plus pions, above threshold. For this reason, we do not dwell on a more precise analysis of this bound, or on a separation into definite isospin channels.

## 4 Proton charge radius extraction

We consider several possibilities to reduce the error bars for the proton charge radius extracted in Section 2. We first consider the inclusion of higher- $Q^2$  data. We then optimize the charge radius extraction by separating isoscalar and isovector components, recognizing that the isoscalar threshold is at  $9m_\pi^2$ . At the same time, we illustrate the (small) effect of different expansion schemes. Finally, we consider the possibility to effectively raise the isovector threshold by constraining the spectral function between  $4m_\pi^2$  and  $16m_\pi^2$ .

### 4.1 Including higher $Q^2$ data

We have argued that, taking the data tabulated in [19] at face value, the final entry in Table 1 is a model-independent determination of the proton charge radius:  $r_E^p = 0.878_{-0.062}^{+0.039} \text{ fm}$ . In the absence of further model-independent constraints on the form factors, obtaining a proton charge radius with smaller error requires further experimental input. Here we investigate the impact of higher- $Q^2$  proton scattering data.

Figure 3 shows the central value and  $1\sigma$  ( $\Delta\chi^2 = 1$ ) error band obtained by fitting the electron-proton scattering data compiled by Arrington et al. [7]. We take  $\phi = 1$  and  $t_0 = 0$ , and include as many coefficients  $a_k$  as necessary for the fits to stabilize. As the figure illustrates, for  $Q^2 \gtrsim \text{few} \times 0.1 \text{ GeV}^2$  the impact of additional data is minimal. While an ever greater number of coefficients  $a_k$  at higher  $k$  must be included to obtain convergence, the total error on the slope at  $Q^2 = 0$  is not reduced. For later use, we note that the coefficients  $a_{k=1,2,3}$  extracted from the fit at  $Q_{\text{max}}^2 = 1 \text{ GeV}^2$  are  $-1.01(6)$ ,  $-1.4_{-0.7}^{+1.1}$ ,  $2_{-6}^{+2}$ .

### 4.2 Raising the isoscalar threshold: inclusion of neutron data

We can separate the isoscalar from the isovector form factor, making use of the fact that the isoscalar cut is further away from  $t = 0$  than the isovector cut, translating to a smaller value

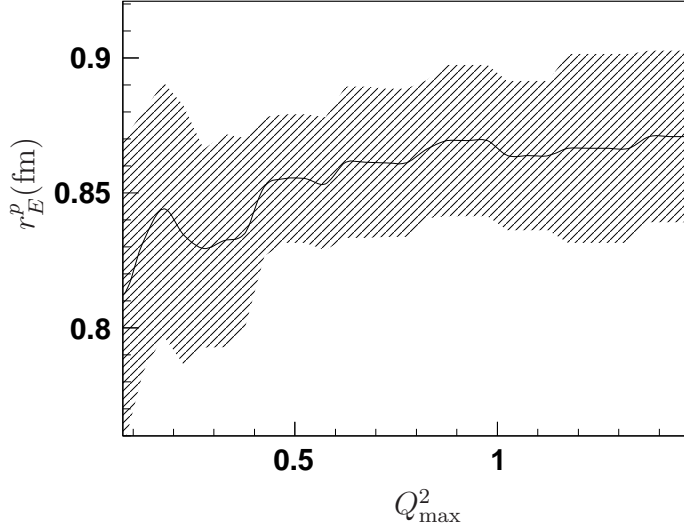


Figure 3: Variation of the fitted proton charge radius as a function of maximum  $Q^2$ . Fits of the proton data were performed with  $k_{\max} = 10$ ,  $\phi = 1$ ,  $t_0 = 0$ ,  $|a_k| \leq 10$ . Data from [7].

of  $|z|_{\max}$  as discussed in the Introduction. A combined fit of proton and neutron data can then be performed. For the proton form factor we again use the data from [7]. For the neutron electric form factor, we use 20 data points from [35, 36, 37, 38, 39, 40, 41, 42, 43, 44, 45, 46]. We take as additional input the neutron charge radius from neutron-electron scattering length measurements [5]:

$$\langle r^2 \rangle_E^n = -0.1161(22) \text{ fm}^2. \quad (31)$$

Table 3 shows the effect of different expansion schemes (choices of  $\phi$  and  $t_0$ ) and coefficient bounds on the form factor slope determination. For later use, the coefficients  $a_{k=1,2,3}$  extracted from the fit for  $Q_{\max}^2 = 1 \text{ GeV}^2$ ,  $\phi = 1$ ,  $t_0 = 0$  and  $k_{\max} = 8$  are  $-1.99^{+0.13}_{-0.12}$ ,  $0.3^{+1.5}_{-1.9}$ ,  $-2^{+9}_{-6}$  for the isoscalar channel; and  $-1.20^{+0.06}_{-0.05}$ ,  $-0.6^{+1.3}_{-1.2}$ ,  $-2^{+6}_{-7}$  for the isovector channel. The sign and approximate magnitude of the first coefficients agree with the  $\pi\pi$  continuum model, and the narrow-width  $\omega$  resonance model mentioned in Section 3.4.

### 4.3 Raising the isovector threshold: inclusion of $\pi\pi$ data

We can effectively raise the isovector threshold by including the  $\pi\pi$  continuum explicitly, as constrained by  $\pi\pi$  production and  $\pi\pi \rightarrow N\bar{N}$  data:

$$G_E^{(1)}(t) = G_{\text{cut}}(t) + \sum_k a_k z^k(t, t_{\text{cut}} = 16m_\pi^2, t_0), \quad (32)$$

where  $G_{\text{cut}}(t)$  is generated by (21) for  $4m_\pi^2 < t < 16m_\pi^2$ . For  $|F_\pi(t)|$  we take the four  $t$  values close to production threshold from [27] (0.101 to 0.178  $\text{GeV}^2$ ), and twelve  $t$  values

	$k_{\max} = 2$	3	4	5	6
$\phi = 1, t_0 = 0,  a_k  \leq 10$	$888_{-5}^{+5}$	$865_{-11}^{+11}$	$888_{-22}^{+17}$	$882_{-22}^{+21}$	$878_{-19}^{+20}$
	$\chi^2 = 33.67$	23.65	21.80	21.13	20.47
$\phi = 1, t_0 = 0,  a_k  \leq 5$	$888_{-5}^{+5}$	$865_{-11}^{+11}$	$881_{-16}^{+10}$	$885_{-21}^{+16}$	$882_{-20}^{+18}$
	$\chi^2 = 33.67$	23.65	21.95	21.46	21.06
$\phi = \phi_{\text{VMD}}, t_0 = 0,  a_k  \leq 10$	$865_{-6}^{+6}$	$874_{-13}^{+12}$	$884_{-24}^{+23}$	$879_{+22}^{+24}$	$877_{-20}^{+22}$
	$\chi^2 = 23.26$	22.50	22.15	21.59	21.09
$\phi = 1, t_0 = 0$	$888_{-5}^{+5}$	$865_{-11}^{+11}$	$880_{-16}^{+13}$	$882_{-18}^{+14}$	$882_{-18}^{+15}$
	$\chi^2 = 33.67$	23.65	22.07	21.45	21.18
$\phi = \phi_{\text{OPE}}, t_0 = 0$	$904_{-5}^{+5}$	$861_{-11}^{+10}$	$888_{-21}^{+14}$	$883_{-20}^{+20}$	$881_{-19}^{+20}$
	$\chi^2 = 61.34$	24.38	21.62	20.86	20.51
$\phi = \phi_{\text{OPE}}, t_0 = t_0^{\text{opt}}(0.5 \text{ GeV}^2)$	$912_{-5}^{+5}$	$869_{-9}^{+9}$	$887_{-19}^{+18}$	$881_{-19}^{+20}$	$880_{-19}^{+20}$
	$\chi^2 = 93.69$	22.54	21.05	20.32	20.32

Table 3: RMS charge radius extracted using electron-proton and electron-neutron scattering data, and different schemes presented in the text. The neutron form factor slope is constrained using (31). A cut  $Q_{\max}^2 = 0.5 \text{ GeV}^2$  is enforced. In the lower part of the table, the bounds on  $\sum_k a_k^2$  from Table 2 are multiplied by 4.  $\phi_{\text{VMD}}$  and  $\phi_{\text{OPE}}$  are defined in Eqs.(22),(23).

from [28] (0.185 to 0.314  $\text{GeV}^2$ ). The product of the remaining kinematic factor and  $f_+^1$  from [29] is interpolated to the appropriate  $t$  value, and the integral computed as a discrete sum. Using coarser bin size (e.g. 8 instead of 16 bins) has no significant effect, indicating that discretization error is small. Estimating the remaining coefficients by modeling the  $\pi\pi$  continuum contribution for  $16m_\pi^2 \leq t \leq 40m_\pi^2$  using (15) and (21) at  $\phi = 1$  and  $t_0 = 0$  gives coefficients  $a_1 \approx -4.5$ ,  $a_2 \approx 2.2$ ,  $a_3 \approx 2.1$ . Setting  $|\sin(k\theta)|$  in (15) yields  $|a_k| \lesssim 5.0$  for the remaining contribution of the  $\pi\pi$  continuum in this model.

We fit using the same proton and neutron data as in Section 4.2. The resulting fit coefficients  $a_{k=1,2,3}$  for  $Q_{\max}^2 = 1 \text{ GeV}^2$ ,  $\phi = 1$ ,  $t_0 = 0$  and  $k_{\max} = 8$  are  $-1.93(6)$ ,  $-0.5_{-1.3}^{+1.1}$ ,  $2 \pm 7$  for the isoscalar form factor; and  $-3.40_{-0.10}^{+0.09}$ ,  $3.7_{-1.3}^{+1.7}$ ,  $3_{-10}^{+5}$  for the isovector form factor. The sign and approximate magnitude of the first coefficients agree with the remaining  $\pi\pi$  continuum model discussed above in the isovector case; and with the  $\omega$  pole model discussed at the end of Section 3.4 for the isoscalar case. The sizable contribution of the isovector  $a_{k=1}$  in this scheme can be traced to the residual effects of the  $\pi\pi$  continuum, including the  $\rho$  peak, near the higher threshold. With no loss of model-independence, we can replace  $G_{\text{cut}}(t)$  above with a new  $G_{\text{cut}}(t)$  generated by (21) for  $4m_\pi^2 < t < 40m_\pi^2$ , i.e., with the  $\pi\pi$  continuum modeled to larger  $t$ . The value  $t_{\text{cut}} = 16m_\pi^2$  remains the same. We emphasize that this does not introduce a model dependence, as any discrepancy between  $G_{\text{cut}}(t)$  and the true  $\pi\pi$  continuum is accounted for by parameters in the  $z$  expansion. The resulting central value and errors on the charge radius are changed minimally by this modification. The isoscalar coefficients are also not significantly changed, while the isovector coefficients become  $1.07(10)$ ,  $1.6_{-1.5}^{+1.6}$ ,  $1_{-8}^{+7}$ .

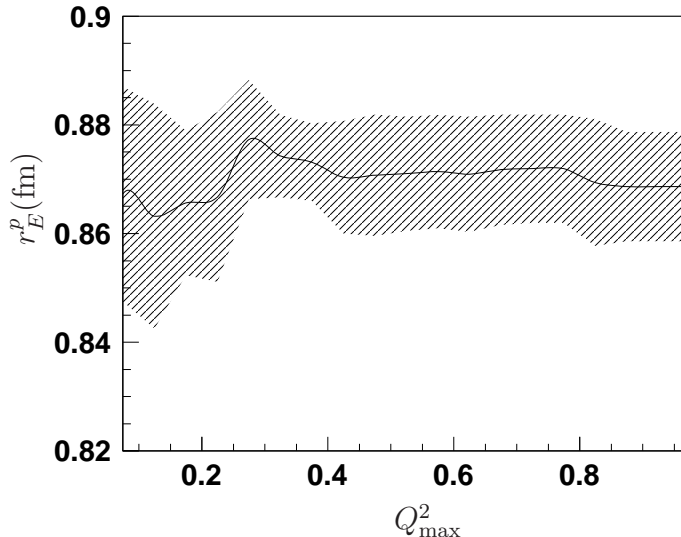


Figure 4: Variation of the fitted proton charge radius as a function of maximum  $Q^2$ . Fits were performed including proton data, neutron data and the  $\pi\pi$  continuum contribution to the isovector spectral function, as detailed in the text. Fits were performed with  $k_{\max} = 8$ ,  $\phi = 1$ ,  $t_0 = 0$ ,  $|a_k| \leq 10$ .

Figure 4 shows the resulting extraction of the proton charge radius using for  $G_{\text{cut}}(t)$  the full model of the  $\pi\pi$  continuum, and our default  $\phi = 1$ ,  $t_0 = 0$ . As in Fig. 3, the inclusion of data beyond  $Q^2 \sim \text{few} \times 0.1 \text{ GeV}^2$  has minimal impact on the fits.

## 5 Discussion

We have discussed determinations of the proton charge radius from the slope of the proton form factor  $G_E^p(t)$ , in four cases: (1) low- $Q^2$  electron-proton scattering data; (2) proton data including high  $Q^2$ ; (3) proton plus neutron data; and (4) proton, neutron, and  $\pi\pi$  data. We have investigated various expansion schemes, corresponding to choices of the parameter  $t_0$  and the function  $\phi$ , and shown that the impact on  $r_E^p$  is minimal; in the following discussion we take  $\phi = 1$  and  $t_0 = 0$ .

Including just the low  $Q^2$  proton data [19], we find the result as in Table 1 [case (1)]  $r_E^p = 0.877^{+0.031}_{-0.049} \pm 0.011 \text{ fm}$ , where the first error is obtained using the more stringent bound  $|a_k| \leq 5$ , and the additional error is conservatively estimated by finding the maximum variation of the  $\Delta\chi^2 = 1$  interval when the fits are redone assuming  $|a_k| \leq 10$ . Using a larger  $Q^2$  range of proton data [7] decreases the uncertainty. Taking for definiteness  $Q_{\max}^2 = 0.5 \text{ GeV}^2$  and  $k_{\max} = 8$ , we obtain via the same procedure, as in Fig. 3 [case (2)]  $r_E^p = 0.870 \pm 0.023 \pm 0.012 \text{ fm}$ . Including the neutron data, as in Table 3, we find [case (3)]  $r_E^p = 0.880^{+0.017}_{-0.020} \pm 0.007 \text{ fm}$ , where the same bounds,  $|a_k| \leq 5$ ,  $|a_k| \leq 10$  are enforced on both isoscalar and isovector

coefficients and again  $k_{\max} = 8$ .<sup>8</sup> The uncertainty induced by the neutron charge radius (31) is negligible in comparison,  $\lesssim 0.0005$  fm. Finally, including  $G_{\text{cut}}(t)$  as in (32), we find [case (4)]  $r_E^p = 0.871 \pm 0.009 \pm 0.002 \pm 0.002$  fm. For definiteness, we here include in  $G_{\text{cut}}(t)$  the extension of the  $\pi\pi$  continuum model up to  $t = 40 m_\pi^2$ . The first and the second error are as above, and the final error is obtained by assigning a 30% normalization error to the continuum contribution, as discussed below.

Let us compare our results to several previous determinations of  $r_E^p$ . Many of these suffer from model assumptions on the functional behavior of the form factor. The small uncertainties obtained by Simon et al. [47] ( $r_E^p = 0.862 \pm 0.012$ ) and by Rosenfelder [19] ( $r_E^p = 0.880 \pm 0.015$ ) require inputs from higher  $Q^2$  data, which however we do not believe were robustly estimated. We find that the coefficient of  $t^2$  in the expansion of  $G_E^p(t)$  [Eq.(4)] is constrained by the Arrington et al. data compilation [7] to be  $a_2^{\text{Taylor}}/t_{\text{cut}}^2 = 0.014_{-0.013}^{+0.016} \pm 0.005$  fm<sup>4</sup> (using  $Q_{\max}^2 = 1$  GeV<sup>2</sup>,  $k_{\max} = 10$ ). A much smaller uncertainty,  $a_2^{\text{Taylor}}/t_{\text{cut}}^2 = 0.011(4)$  fm<sup>4</sup> or  $0.014(4)$  fm<sup>4</sup>, was adopted in [19]. Even neglecting the additional uncertainty due to cubic and higher order terms, this would lead to a result  $0.878 \pm 0.008_{-0.039}^{+0.047}$  obtained using (4) and data as in Table 1. The errors are from the data and from the first uncertainty on the quadratic coefficient, respectively.

The analyses of Sick [20] ( $r_E^p = 0.895 \pm 0.010 \pm 0.013$ ) and Blunden and Sick [48] ( $r_E^p = 0.897 \pm 0.018$ ) employ the continued fraction expansion (5). This functional form is unstable to the inclusion of additional parameters (see Table 1), and error estimation relies on the investigation of model datasets. In this paper we have not fit directly to cross section data, and we have not applied our analysis to this dataset. For a variation of this analysis see [49].

The dispersion analysis of Belushkin et al. [26] ( $r_E^p = 0.844_{-0.004}^{+0.008}$  fm,  $r_E^p = 0.830_{-0.008}^{+0.005}$ ) does not attempt to estimate uncertainties due to the constrained shape of the assumed form factors. Our analysis makes clear which inputs have the most effect on the charge radius extractions. In particular, data at large  $|t|$ , for either timelike or spacelike  $t$ , has minimal impact on fits to obtain  $Q^2 \approx 0$  quantities. Inclusion of high- $Q^2$  data *does* introduce sensitivity to additional parameters, whose omission would introduce model dependence. Our analysis provides a systematic procedure to analyze a wide range of datasets in a model-independent way. We emphasize that our goal is not simply reduction in the quoted error, but also the robust estimation of uncertainties.

Regarding the bounds on coefficients, in all approximations that we have considered the bound  $|a_k| \leq 10$  appears very conservative. The sign and magnitudes of the first coefficients are consistent with expectations based on simple models, and it is rigorously true that the coefficients  $a_k$  must eventually decrease in magnitude for large  $k$ . At a practical level, the experimental determinations of these coefficients in each of the cases (1)-(4) above are consistent with magnitudes not larger than  $|a_k| \sim 2$ . Our implementation of the bounds on  $a_k$  could be formalized in terms of standard methods of constrained curve fitting [50]. As discussed in [15], our assumption of a flat “prior” should be conservative.

Our analysis cannot discern inaccuracies in the datasets. For example, we have assumed that radiative corrections are properly accounted for in the compilations [19, 7], and that

---

<sup>8</sup> The slight difference between this value and that inferred from the final column for the first two rows of Table 3 is due to the slight difference between  $k_{\max} = 6$  and  $k_{\max} = 8$ .

data correlations are sufficiently described by our treatment.<sup>9</sup> Within these assumptions, the values for cases (1)-(3) represent model-independent determinations of the form-factor slope. Case (4) is more subtle. While (21) is a model-independent relation for the stated range  $4m_\pi^2 \leq t \leq 16m_\pi^2$ , the determination of  $f_+^1(t)$  in this range involves a dispersion relation with contributions from values of  $t$  where the function is not rigorously constrained by continuation of  $\pi N$  scattering data. Errors are not given in the tabulation [29], and we are not aware of a critical assessment of the uncertainties associated with this analysis. It may be interesting to revisit this question. Ref. [24] suggests a 15% error in the normalization of  $f_+^1(t)$  at the  $\rho$  peak; we take twice this value, 30%, as a representative uncertainty, which encompasses also the errors in  $|F_\pi(t)|$ . The resulting error for case (4) is thus not as rigorous, although the resulting  $f_+^1(t)$  would need to be very different to become a dominant source of error.

Within the stated uncertainties we find consistent results in each of our determinations, using both low and high  $Q^2$  proton data, neutron data, and pion continuum data. These methods can be applied to other datasets, and to fits using partial cross sections versus extracted form factors. For example, in a recent set of results [53] the variation of  $r_E^p$  under different model shapes for the form factor is larger than the other stated statistical and systematic errors. The same methods can be applied to other nucleon form factors and derived observables, including the axial-vector form factor probed in neutrino scattering [54].

## Acknowledgements

We have benefited from discussions with Z.-T. Lu and C. E. M. Wagner. We also thank J. Arrington for discussions and comments on the manuscript. This work is supported by NSF Grant 0855039 and DOE grant DE-FG02-90ER40560.

## References

- [1] T. Udem, A. Huber, B. Gross, J. Reichert, M. Prevedelli, M. Weitz and T. W. Hansch, Phys. Rev. Lett. **79**, 2646 (1997).
- [2] K. Melnikov and T. van Ritbergen, Phys. Rev. Lett. **84**, 1673 (2000) [arXiv:hep-ph/9911277].
- [3] R. Pohl *et al.*, Nature **466**, 213 (2010).
- [4] P. J. Mohr, B. N. Taylor and D. B. Newell, Rev. Mod. Phys. **80**, 633 (2008) [arXiv:0801.0028 [physics.atom-ph]].
- [5] K. Nakamura *et al.* [Particle Data Group], J. Phys. G **37**, 075021 (2010).
- [6] P. Federbush, M. L. Goldberger and S. B. Treiman, Phys. Rev. **112**, 642 (1958).
- [7] J. Arrington, W. Melnitchouk and J. A. Tjon, Phys. Rev. C **76**, 035205 (2007) [arXiv:0707.1861 [nucl-ex]].

---

<sup>9</sup> Two-photon exchange corrections were incorporated in [19] using a simplified calculation of the Coulomb distortion. See also [20, 48]. Ref. [7] accounted for two-photon exchange using the calculation of [51, 52].



- [8] For a review and further references see: R. J. Hill, *In the Proceedings of 4th Flavor Physics and CP Violation Conference (FPCP 2006), Vancouver, British Columbia, Canada, 9-12 Apr 2006, pp 027* [arXiv:hep-ph/0606023].
- [9] C. Bourrely, B. Machet and E. de Rafael, Nucl. Phys. B **189**, 157 (1981).
- [10] C. G. Boyd, B. Grinstein and R. F. Lebed, Phys. Rev. Lett. **74**, 4603 (1995) [arXiv:hep-ph/9412324].
- [11] C. G. Boyd, B. Grinstein and R. F. Lebed, Nucl. Phys. B **461**, 493 (1996) [arXiv:hep-ph/9508211].
- [12] L. Lellouch, Nucl. Phys. B **479**, 353 (1996) [arXiv:hep-ph/9509358].
- [13] I. Caprini, L. Lellouch and M. Neubert, Nucl. Phys. B **530**, 153 (1998) [arXiv:hep-ph/9712417].
- [14] M. C. Arnesen, B. Grinstein, I. Z. Rothstein and I. W. Stewart, Phys. Rev. Lett. **95**, 071802 (2005) [arXiv:hep-ph/0504209].
- [15] T. Becher and R. J. Hill, Phys. Lett. B **633**, 61 (2006) [arXiv:hep-ph/0509090].
- [16] R. J. Hill, Phys. Rev. D **74**, 096006 (2006) [arXiv:hep-ph/0607108].
- [17] C. Bourrely, I. Caprini and L. Lellouch, Phys. Rev. D **79**, 013008 (2009) [arXiv:0807.2722 [hep-ph]].
- [18] A. Bharucha, T. Feldmann and M. Wick, JHEP **1009**, 090 (2010) [arXiv:1004.3249 [hep-ph]].
- [19] R. Rosenfelder, Phys. Lett. B **479**, 381 (2000) [arXiv:nucl-th/9912031].
- [20] I. Sick, Phys. Lett. B **576**, 62 (2003) [arXiv:nucl-ex/0310008].
- [21] L. L. Foldy, Phys. Rev. **87**, 688 (1952).
- [22] G. Salzman, Phys. Rev. **99**, 973 (1955).
- [23] F. J. Ernst, R. G. Sachs and K. C. Wali, Phys. Rev. **119**, 1105 (1960).
- [24] G. Hohler and E. Pietarinen, Nucl. Phys. B **95**, 210 (1975).
- [25] W. R. Frazer and J. R. Fulco, Phys. Rev. **117**, 1609 (1960).
- [26] M. A. Belushkin, H. W. Hammer and U. G. Meissner, Phys. Rev. C **75**, 035202 (2007) [arXiv:hep-ph/0608337].
- [27] S. R. Amendolia *et al.*, Phys. Lett. B **138**, 454 (1984).
- [28] M. N. Achasov *et al.*, J. Exp. Theor. Phys. **101**, 1053 (2005) [Zh. Eksp. Teor. Fiz. **101**, 1201 (2005)] [arXiv:hep-ex/0506076].

- [29] G. Höhler, Pion-nucleon scattering, in: H. Schopper (editor), Landolt-Börnstein database, Volume 9, subvolume b, part 1, Springer-Verlag, Berlin, 1983. [<http://www.springermaterials.com/navigation/>]
- [30] N. Cabibbo and R. Gatto, Phys. Rev. **124**, 1577 (1961).
- [31] M. Ablikim *et al.* [BES Collaboration], Phys. Lett. B **630**, 14 (2005) [arXiv:hep-ex/0506059].
- [32] T. K. Pedlar *et al.* [CLEO Collaboration], Phys. Rev. Lett. **95**, 261803 (2005) [arXiv:hep-ex/0510005].
- [33] B. Aubert *et al.* [BABAR Collaboration], Phys. Rev. D **73**, 012005 (2006) [arXiv:hep-ex/0512023].
- [34] A. Antonelli *et al.*, Nucl. Phys. B **517**, 3 (1998).
- [35] J. Bermuth *et al.*, Phys. Lett. B **564**, 199 (2003) [arXiv:nucl-ex/0303015].
- [36] T. Eden *et al.*, Phys. Rev. C **50**, R1749 (1994).
- [37] E. Geis *et al.* [BLAST Collaboration], Phys. Rev. Lett. **101**, 042501 (2008) [arXiv:0803.3827 [nucl-ex]].
- [38] D. I. Glazier *et al.*, Eur. Phys. J. A **24**, 101 (2005) [arXiv:nucl-ex/0410026].
- [39] J. Golak, G. Ziener, H. Kamada, H. Witala and W. Gloeckle, Phys. Rev. C **63**, 034006 (2001) [arXiv:nucl-th/0008008].
- [40] C. Herberg *et al.*, Eur. Phys. J. A **5**, 131 (1999).
- [41] M. Ostrick *et al.*, Phys. Rev. Lett. **83**, 276 (1999).
- [42] I. Passchier *et al.*, Phys. Rev. Lett. **82**, 4988 (1999) [arXiv:nucl-ex/9907012].
- [43] B. Plaster *et al.* [Jefferson Laboratory E93-038 Collaboration], Phys. Rev. C **73**, 025205 (2006) [arXiv:nucl-ex/0511025].
- [44] D. Rohe *et al.*, Phys. Rev. Lett. **83**, 4257 (1999).
- [45] G. Warren *et al.* [Jefferson Lab E93-026 Collaboration], Phys. Rev. Lett. **92**, 042301 (2004) [arXiv:nucl-ex/0308021].
- [46] H. Zhu *et al.* [E93026 Collaboration], Phys. Rev. Lett. **87**, 081801 (2001) [arXiv:nucl-ex/0105001].
- [47] G. G. Simon, C. Schmitt, F. Borkowski and V. H. Walther, Nucl. Phys. A **333**, 381 (1980).
- [48] P. G. Blunden and I. Sick, Phys. Rev. C **72**, 057601 (2005) [arXiv:nucl-th/0508037].

- [49] D. Borisyuk, Nucl. Phys. A **843**, 59 (2010) [arXiv:0911.4091 [hep-ph]].
- [50] For an introduction, see: G. P. Lepage, B. Clark, C. T. H. Davies, K. Hornbostel, P. B. Mackenzie, C. Morningstar and H. Trottier, Nucl. Phys. Proc. Suppl. **106**, 12 (2002) [arXiv:hep-lat/0110175]. For a related discussion see: M. R. Schindler and D. R. Phillips, Annals Phys. **324**, 682 (2009) [Erratum-ibid. **324**, 2051 (2009)] [arXiv:0808.3643 [hep-ph]].
- [51] P. G. Blunden, W. Melnitchouk and J. A. Tjon, Phys. Rev. Lett. **91**, 142304 (2003) [arXiv:nucl-th/0306076].
- [52] P. G. Blunden, W. Melnitchouk and J. A. Tjon, Phys. Rev. C **72**, 034612 (2005) [arXiv:nucl-th/0506039].
- [53] J. C. Bernauer *et al.* [A1 Collaboration], arXiv:1007.5076 [nucl-ex].
- [54] R. J. Hill and G. Paz, in preparation.